BENCHMARK OSIRIS QED PROCESSES

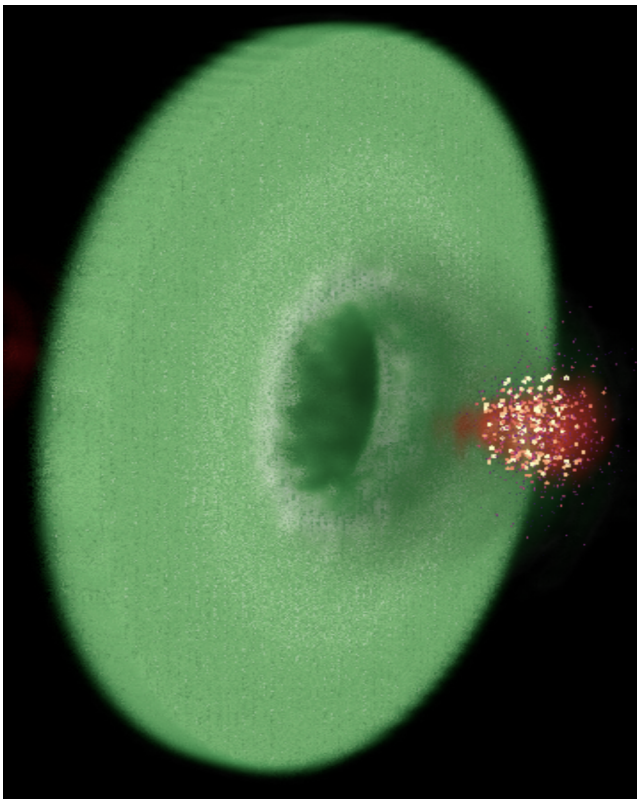

Author
B. Martinez
Instituto Superior Técnico, Universidade de Lisboa
July 2023

Introduction

In this document, we benchmark the recently implemented QED processes in Osiris. For each process, we recall the theoretical cross-section [1, 2], how it is implemented and validate the Monte Carlo module added in Osiris.

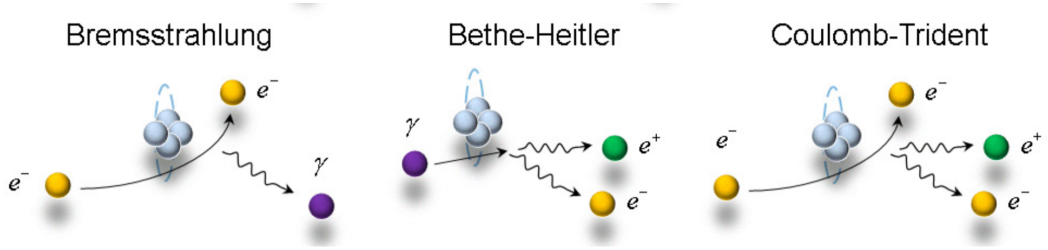

Figure 1: QED processes recently implemented in the code Osiris (a) Bremsstrahlung emission of γ-rays (b) Bethe-Heitler pair production (c) Coulomb Trident pair production.

Contents

1 Bremsstrahlung emission of gamma-rays

There is no single formula for the Bremsstrahlung cross-section. However, there are formulas for different regimes (i) the non-relativistic regime ($1 < \gamma_1 < 2$) (ii) the midly relativistic regime ($2 < \gamma_1 < 100$) (iii) the ultra-relativistic regime ($100 < \gamma_1$). The Bremsstrahlung cross-sections are derived with three assumptions: (i) the atom is isolated (ii) the atom is at rest (iii) the atom potential is given by the Thomas-Fermi potential $V(r) = Ze/(4\pi\epsilon_0 r)e^{-r/\lambda_{tf}}$, with λ_{tf} the Thomas-Fermi length defined as $\lambda_{tf} = 4\pi\epsilon_0\hbar^2 Z^{-1/3}/(mc^2)$. We introduce $\widetilde{V}(\mathbf{u})$ the Fourier transform of $V_{\rm tf}(\mathbf{r})$, normalized by the factor $e/(\alpha_f m_e c^2)$

$$\widetilde{V}(\mathbf{u}) = \frac{1}{(2\pi)^3}\int \frac{eV_{tf}(\mathbf{r})}{\alpha_f m_e c^2}\exp\left(i\frac{\mathbf{u}\cdot\mathbf{r}}{r_{\rm C}}\right) d^3\left(\frac{\mathbf{r}}{r_{\rm C}}\right), \tag{1}$$

with $r_C = \hbar/mc$ the Compton radius.

Let us consider an electron of total energy $E_1/m_e c^2 = \gamma_1$, normalized momentum $p_1 = \sqrt{\gamma_1^2 - 1}$, normalized velocity β_1 both measured in the atom rest frame, with an atomic number Z. After emitting a photon of normalized energy $k = \hbar\omega/m_e c^2$ in the screened atomic field, the normalized electron energy $\gamma_2 = \gamma_1 - k$, a momentum $p_2 = \sqrt{\gamma_2^2 - 1}$ and a velocity β_2. We introduce the notation $\delta p_\pm = p_1 \pm p_2$. The fine structure constant is denoted α_f and the classical electron radius r_e.

1.1 Theoretical cross-section

Non-relativistic Bremsstrahlung cross-section The non-relativistic ($1 < \gamma_1 < 2$) Bremsstrahlung cross section is given in the Born approximation in Ref [3]

$$\frac{d\sigma_{\rm br,nr}}{dk} = \frac{16 r_e^2 Z^2 \alpha_f}{3kp_1^2}\frac{1}{2}\left[\ln\left(\frac{\delta p_+^2\lambda_{tf}^2 + 1}{\delta p_-^2\lambda_{tf}^2 + 1}\right) + \frac{1}{\delta p_+^2\lambda_{tf}^2 + 1} - \frac{1}{\delta p_-^2\lambda_{tf}^2 + 1}\right] \tag{2}$$

It is established [4] that the accuracy of the Born approximation can be improved in the non-relativistic regime by multiplying Eq. (2) by the Elwert correction factor [4, 5]:

$$f_{\rm E} = \frac{\beta_1}{\beta_2}\frac{1 - \exp\left(-2\pi Z\alpha_f/\beta_1\right)}{1 - \exp\left(-2\pi Z\alpha_f/\beta_2\right)}. \tag{3}$$

This correction is valid in the limit where $Z\alpha_f(1/\beta_2 - 1/\beta_1) \ll 1$. In practise, we will apply this factor when $Z\alpha_f(1/\beta_2 - 1/\beta_1) \leq 0.01$. It corrects the divergence of the differential cross-section only at high photon energies, therefore introducing a slight discontinuity.

Moderately-relativistic Bremsstrahlung cross-section For moderately relativistic electrons ($2 \leq \gamma_1 \leq 100$), the photon-energy-differential Bremsstrahlung cross section is given by the following expression, valid for arbitrary screening [6, 7]:

$$\frac{d\sigma_{\rm br,mr}}{dk} = \frac{4Z^2 r_e^2 \alpha_f}{k}\left[1 + \left(\frac{\gamma_1 - k}{\gamma_1}\right)^2\right](I_1(\delta) + 1) - \frac{2}{3}\frac{\gamma_1 - k}{\gamma_1}\left(I_2(\delta) + \frac{5}{6}\right) \tag{4}$$

where the functions I_1 and I_2 account for screening effects:

$$I_1(\delta) = \int_\delta^1 \frac{du}{u^3} (u-\delta)^2 \left[1 - F_e(u)\right]^2 , \tag{5}$$

$$I_2(\delta) = \int_\delta^1 \frac{du}{u^4} \left[u^3 - 6\delta^2 u \ln(u/\delta) + 3\delta^2 u - 4\delta^3\right] \times \left[1 - F_e(u)\right]^2 . \tag{6}$$

The argument $\delta = k/2\gamma_1(\gamma_1 - k)$ approximately measures the minimum momentum transfer to the atom in the limit $\gamma_1, \gamma_2 \gg 1$. The above functions involve the atomic form factor

$$1 - F_e(u) = \frac{2\pi^2}{Z} u^2 \widetilde{V}(u) . \tag{7}$$

For a simple single-exponential atomic potential, $V(r) = Ze/(4\pi\epsilon_0 r)e^{-r/\lambda_{tf}}$, the integrals I_1 and I_2 can be exactly calculated:

$$I_1 = \lambda_{tf}\delta \left(\arctan\left(\delta\lambda_{tf}\right) - \arctan\lambda_{tf}\right) - \frac{\lambda_{tf}^2}{2}\frac{(1-\delta)^2}{1+\lambda_{tf}^2} + \frac{1}{2}\ln\left(\frac{1+\lambda_{tf}^2}{1+\lambda_{tf}^2\delta^2}\right) , \tag{8}$$

$$\begin{aligned} 2I_2 = {} & 4\lambda_{tf}^3\delta^3 \left(\arctan(\delta\lambda_{tf}) - \arctan(\lambda_{tf})\right) + \left(1 + 3\lambda_{tf}^2\delta^2\right)\ln\left(\frac{1+\lambda_{tf}^2}{1+\lambda_{tf}^2\delta^2}\right) \\ & + \frac{6\lambda_{tf}^4\delta^2}{1+\lambda_{tf}^2}\ln\delta + \frac{\lambda_{tf}^2(\delta-1)\left(\delta + 1 - 4\lambda_{tf}^2\delta^2\right)}{1+\lambda_{tf}^2} . \end{aligned} \tag{9}$$

Ultra-relativistic Bremsstrahlung cross-section For ultra-relativistic electron energies ($\gamma_1 > 100$), the accuracy of the Born-approximation formula (4) can be improved by adding the Coulomb correction term $-f_{\mathrm{C}}(Z)$ as follows [7]:

$$\begin{aligned} \frac{d\sigma_{Br,ur}}{dk} = \frac{4Z^2 r_e^2 \alpha_f}{k} \Bigg\{ & \left[1 + \left(\frac{\gamma_1 - k}{\gamma_1}\right)^2\right] \left[I_1(\delta) + 1 - f_{\mathrm{C}}(Z)\right] \\ & - \frac{2}{3}\frac{\gamma_1 - k}{\gamma_1}\left[I_2(\delta) + \frac{5}{6} - f_{\mathrm{C}}(Z)\right]\Bigg\} , \end{aligned} \tag{10}$$

Introducing the Riemann function ζ, the Coulomb correction term is defined as [7]

$$f_{\mathrm{C}}(Z) = \frac{\alpha_f^2 Z^2}{1+\alpha_f^2 Z^2} \sum_{n=0}^{\infty} \left(-\alpha_f^2 Z^2\right)^n \left[\zeta(2n+1) - 1\right] . \tag{11}$$

In practice, keeping the first four terms has been found sufficient for an accurate computation of f_{C} even for high Z values.

1.2 Algorithm and tables

Algorithm The routine for Bremsstrahlung of electron/positron is in the particle pusher, just after radiative losses by Inverse Compton scattering. It follows these steps:

- Damp the ion density at the position of the electron/positron
- Compute the probability for an event
- Decides whether the event takes place with a random number

- If it takes place, the photon energy is sampled from the CDF in the table and another random number
- A new photon is created on the grid and the energy of the electron is damped

Table For the Bremsstrahlung process, there is one table per atomic number, and we implemented it for $Z = 13$ and $Z = 29$. The incident kinetic electron energy denoted $\gamma_- - 1$ is in the range $(10^{-3}\, mc^2,\, 4 \times 10^4\, mc^2)$ with a logarithmic step and 70 points. The emitted photon energy denoted k starts at 0 and can be as high as the kinetic energy of the electron $\gamma_- - 1$. As the cross-section diverges for $k \to 0$, it is taken in the range $k/(\gamma_- - 1) \in (10^{-7},\, 1)$ with a logarithmic step and 20 points. The part of the spectrum neglected has a negligible contribution to the total spectrum.

1.3 Exact simulation of photon number and spectra

We performed 2D simulations with periodic conditions along the x and y axes in a domain of size $(4\, c/\omega_0)^2$. We model only one time step so that electrons radiate only once. We consider the propagation of a monoenergetic electron beam with an energy of 40 MeV, density $n_e/n_c = 10^{-4}$ and a surface $S = (4\, c/\omega_0)^2$ through a solid copper target of density $n_i/n_c = 100$. Given the simple system we investigate, the theoretical number of photons is provided by the following formula

$$\frac{dN_k}{dt} = n_e S \times \sigma_{br} n_i v_e \tag{12}$$

where $n_e S$ is the number of electrons per unit of transverse dimension, and $\sigma_{br} n_i v_e$ the frequency of photon emission for one electron. In order to get a real number of photons, we assumed the third dimension to be equal to c/ω_0. The expected photon spectra is obtained from the derivation of Eq. (12) against k the photon energy. The photon energy k is re-scaled in order to range from 0 to 1. Using this theoretical estimate, we have validated the spectra simulated by Osiris for various incident electron energies in Fig. 2.

We note that the range of photon energies described extends on 8 orders of magnitude, thanks to the logarithmic step in the table. Although the code can model the creation of such low-energy photons, it cannot model their propagation consistently. In practise, we would allow the propagation of high-energy photons, which wavelength cannot be discribed by the PIC grid.

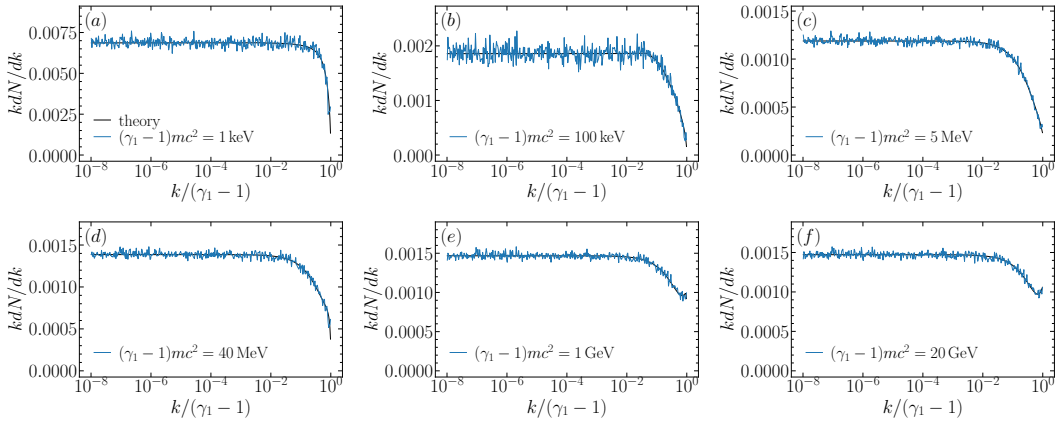

Figure 2: Bremsstrahlung γ-ray production in Osiris for different incident electron energies in Copper ($Z = 29$) (a) 1 keV (b) 100 keV (c) 5 MeV (d) 40 MeV (e) 1 GeV (f) 20 GeV.

2 Bethe Heitler pair production

2.1 Theoretical cross-section

The cross section of Bethe-Heitler pair production by a photon of normalized energy $k \gg 1$, differential in the normalized positron energy γ_+, is given in the ion-rest frame by formula 3D-1003 of Ref. [8]:

$$\frac{d\sigma_{\mathrm{bh}}}{d\gamma_+} = \frac{4Z^2 r_e^2 \alpha_f}{k^3}\left\{ \left(\gamma_+^2 + \gamma_-^2\right)\left[I_1(\delta)+1\right] + \frac{2}{3}\gamma_+\gamma_-\left[I_2(\delta)+\frac{5}{6}\right]\right\}, \tag{13}$$

where $\delta = k/(2\gamma_+\gamma_-)$. This formula further assumes large electron and positron energies ($\gamma_+, \gamma_- \gg 1$) and negligible nucleus recoil. We note that it bears much resemblance to the relativistic Bremsstrahlung cross section, Eq. (4); in particular, it involves the same screening functions $I_{1,2}$, defined by Eqs. (5) and (6), which we again evaluate using the Thomas-Fermi potential. At high photons energies ($\hbar\omega \gtrsim 100\,\mathrm{MeV}$) a Coulomb correction can also be applied to Eq. (13) (see formula 3D-1009 of Ref. [8] and related discussion in Ref. [9]) using the same additive factor $-f_C$ as in the ultra-relativistic Bremsstrahlung cross section, Eq. (10).

2.2 Algorithm and tables

Algorithm The routine for Bethe Heitler of gamma-rays is in the photon pusher, just after pair creation by Nonlinear Breit-Wheeler pair creation. It follows these steps:

- Damp the ion density at the position of the gamma-ray
- Compute the probability for an event
- Decides whether the event takes place with a random number
- If it takes place, the positron energy is sampled from the CDF in the table and another random number
- A new pair is created on the grid and the gamma-ray is removed from the simulation

Table For the Bethe Heitler process, there is one table per atomic number, and we implemented it for $Z = 13$ and $Z = 29$. The incident photon energy denoted k is in the range $k \in (2.1\,mc^2,\, 4 \times 10^4\,mc^2)$ with a logarithmic step and 40 points. The positron energy denoted γ_+ is sampled in the range $\gamma_+ \in (1,\, k-1)$ with 20 points and a linear step.

2.3 Exact simulation of positron number and spectra

We performed 2D simulations with periodic conditions along the x and y axes in a domain of size $(4\,c/\omega_0)^2$. We model only one time step so that the energy of the pairs created does not change over time. We consider the propagation of a monoenergetic gamma-ray beam with an energy of 10 MeV, density $n_k/n_c = 10^{-4}$ and a surface $S = (4\,c/\omega_0)^2$ through a solid copper target of density $n_i/n_c = 100$. Given the simple system we investigate, the theoretical number of positrons is provided by the following formula

$$\frac{dN_+}{dt} = n_k S \times \sigma_{bh} n_i c \tag{14}$$

where $n_k S$ is the number of gamma-rays per unit of transverse dimension, and $\sigma_{bh} n_i c$ the frequency of positron emission for one gamma-ray. In order to get a real number of positrons, we assumed the third dimension to be equal to c/ω_0. The expected positron spectra is obtained from the derivation of Eq. (14) against γ_+ the positron energy. The positron energy γ_+ is re-scaled in order to range from 0 to 1. Using this theoretical estimate, we have validated the spectra simulated by Osiris for various incident gamma-ray energies in Fig. 3.

We observe a good agreement on the whole parameter range. We note the presence of steps in the spectrum, that come from the discretisation of the table. In Figs 3(a-b), we observe that the spectrum predicted close to the pair creation threshold is correct.

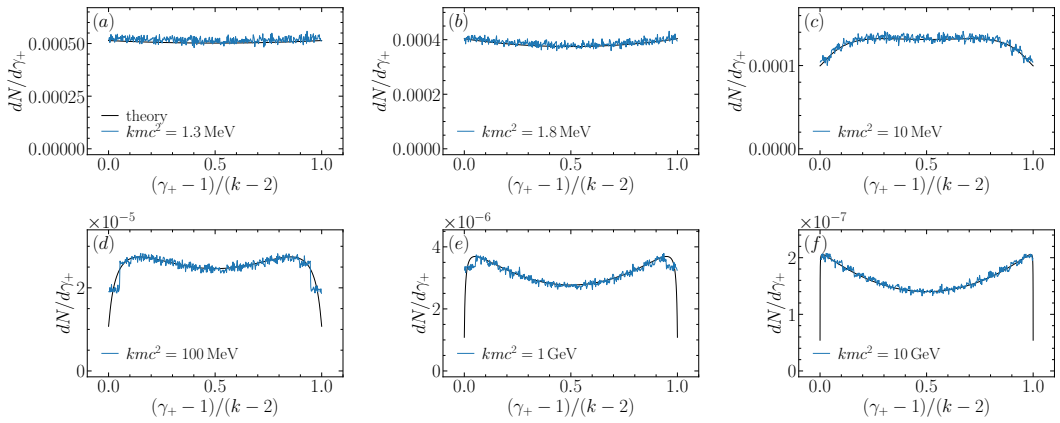

Figure 3: Bethe Heilter pair production in Osiris for different incident electron energies in Copper ($Z = 29$) (a) 1.3 MeV (b) 1.8 MeV (c) 10 MeV (d) 100 MeV (e) 1 GeV (f) 20 GeV.

3 Coulomb Trident pair production

3.1 Theoretical cross-section

The Trident process corresponds to direct pair production by a high-energy electron in the Coulomb field of a nucleus. Due to the lack of tractable analytical formulas, screening effects on this process will be neglected here. Our approach reproduces that adopted by Vodopiyanov *et al.* [10]. Specifically, we use for the total Trident cross section the fitting formula provided by Gryaznykh [11], based on numerical evaluation of the cross section derived by Baier and Fadin [12]:

$$\sigma_{\rm T} = 5.22 Z^2 \ln^3\left(\frac{\gamma_1 + 4.50}{6.89}\right) \times 10^{-34}\,{\rm m}^2\,, \tag{15}$$

where γ_1 is the incident electron's Lorentz factor. It has recently been suggested [13] that this numerical fit may overestimate the exact cross section by a factor of ~ 4. Yet, in the absence of unambiguous theoretical proof, and in line with Refs. [14, 10], we continue using it in its original form. The total (normalized) energy of the created pair ($\gamma_p = \gamma_+ + \gamma_-$) is obtained from the singly differential cross sections calculated by Bhabha [15] in the low- and high-energy limits:

$$\frac{d\sigma_{\rm T,nr}}{d\gamma_p} = \frac{\left(Z r_e \alpha_f\right)^2}{32} \times \left[\log\gamma_1^2 - \frac{161}{60} + C + C_r + C_z\right] \times \frac{E_p^3}{\left(m_e c^2\right)^3}\,, \quad (p_+, p_-) \ll m_e c \tag{16}$$

$$\frac{d\sigma_{\rm T,r}}{d\gamma_p} = \frac{56}{9\pi}\left(Z r_e \alpha_f\right)^2 \ln\left(\frac{C_1 E_p}{m_e c^2}\right) \times \ln\left(\frac{C_2 m_e c^2 \gamma_1}{E_p}\right) \frac{m_e c^2}{E_p}\,, \quad (p_+, p_-) \gg m_e c \tag{17}$$

where C_1 and C_2 are close to unity, and the coefficients C, C_r and C_z are given by

$$\begin{aligned} &C_1 = C_2 = 1 \\ &C = 4\frac{x^2}{1-x^2}\log\frac{1}{x^2} - \frac{4}{3}x^2 + \frac{1}{6}x^4 \\ &C_z = 3\frac{x^2}{1-x^2}\left(1 - \frac{x^2}{1-x^2}\log\frac{1}{x^2}\right) - \frac{13}{5}x^2 + \frac{7}{4}x^4 - \frac{9}{10}x^6 + \frac{1}{5}x^8 \\ &C_r = -\frac{3}{2}\frac{x^2}{1-x^2}\left(1 - \frac{x^2}{1-x^2}\log\frac{1}{x^2}\right) + \frac{4}{5}x^2 - \frac{1}{8}x^4 - \frac{1}{20}x^6 + \frac{1}{40}x^8 \end{aligned} \tag{18}$$

where $x = 1/\gamma_1$. An approximate cross section for arbitrary pair energies is obtained by the simple interpolation formula:

$$\frac{d\sigma_{\rm T}}{d\gamma_p} = \frac{(d\sigma_{\rm T,nr} d\gamma_p)(d\sigma_{\rm T,r}/d\gamma_p)}{d\sigma_{\rm T,nr}/d\gamma_p + d\sigma_{\rm T,r}/d\gamma_p}\,. \tag{19}$$

Knowing the pair energy, the positron (or electron) energy is computed making use of the doubly differential cross section (32) of Ref. [15]:

$$\frac{d\sigma_{\rm T}}{d\gamma_+} \propto \left(\gamma_+^2 + \gamma_-^2 + \frac{2}{3}\gamma_+\gamma_-\right)\ln\frac{\gamma_+\gamma_-}{\gamma_p}\,, \tag{20}$$

where $\gamma_- = \gamma_p - \gamma_+$. As in Ref. [10], we use this generic shape for the positron/electron distribution in the entire energy range even though, in principle, this formula holds only for

$\gamma_1 \gg (\gamma_+, \gamma_-) \gg 1$.

3.2 Algorithm and tables

Algorithm The routine for Coulomb Trident of electrons/positrons is in the particle pusher, just after nonlinear Inverse Compton and Bremsstrahlung routines. It follows these steps:

- Damp the ion density at the position of the electron/positron
- Compute the probability for an event
- Decides whether the event takes place with a random number
- If it takes place, the total pair energy is sampled from the CDF of the single-differential cross-section in pair energy
- The positron energy is then sampled with the double-differential cross-section in pair and positron energy
- The new pair is created on the grid and the energy of the electron is damped.

Table There are three tables for the Coulomb Trident process with (i) the total cross-section (ii) the single-differential cross-section in pair energy (ii) the doubly-differential cross-section in pair and positron energies. The theory is limited to un-screened nucleus, so that the Z-dependence of the cross-sections is trivial ($\propto Z^2$). As such the table for the total cross-section stores σ_{ct}/Z^2 and it is re-scaled at run-time to account for the actual atomic number of the species considered. For the two other tables, the Z^2 dependence simplifies and they also work for any atomic number. The double differential cross-section for this process is derived in the high-energy limit ($\gamma_-, \gamma_\pm, \gamma_+ \gg 1$) and can take negative values close to the pair creation threshold. This can create inconsistencies in the cumulative distribution functions (CDF) tabulated, namely breaking their monotonic behavior and ranging outside $(0, 1)$. To avoid these issues, we choose a generic profile for the CDF of the double-differential cross-section, that is independent on the electron/pair/positron energy.

The incident electron energy denoted γ_- is in the range $(6\,mc^2,\, 4\times10^4\,mc^2)$ with a logarithmic step and 40 points. The pair energy denoted $\gamma_\pm$ is in the range $\gamma_\pm \in (2,\, \gamma_- - 1)$ with 40 points and a logarithmic step. The positron energy denoted γ_+ is in the range $\gamma_+ \in (1,\, \gamma_\pm - 1)$ with 20 points and a linear step.

3.3 Exact simulation of positron number and spectra

We performed 2D simulations with periodic conditions along the x and y axes in a domain of size $(4\,c/\omega_0)^2$. We model only one time step so that electrons create pairs only once. We consider the propagation of a monoenergetic electron beam with an energy of 40 MeV, density $n_e/n_c = 10^{-4}$ and a surface $S = (4\,c/\omega_0)^2$ through a solid copper target of density $n_i/n_c = 100$. Given the simple system we investigate, the theoretical number of pairs is provided by the following formula

$$\frac{dN_p}{dt} = n_e S \times \sigma_{ct} n_i v_e \tag{21}$$

where $n_e S$ is the number of electrons per unit of transverse dimension, and $\sigma_{ct} n_i v_e$ the frequency of pair emission for one electron. In order to get a real number of pairs, we

assumed the third dimension to be equal to c/ω_0. The expected pair spectra is obtained from the derivation of Eq. (21) against γ_p the pair energy. The pair energy $\gamma_p = \gamma_+ + \gamma_-$ is re-scaled in order to range from 0 to 1. Using this theoretical estimate, we have validated the spectra simulated by Osiris for various incident electron energies in Fig. 4.

We observe a good agreement in the whole parameter range at stake. We also note the steps in the distribution of the pair energy, that comes from the discretisation of the table. For high energy incident electrons (1-20 GeV), the peak of the pair spectrum is relatively at low energies (1-10 MeV) but it is still well described thanks to the logarithmic step of the table.

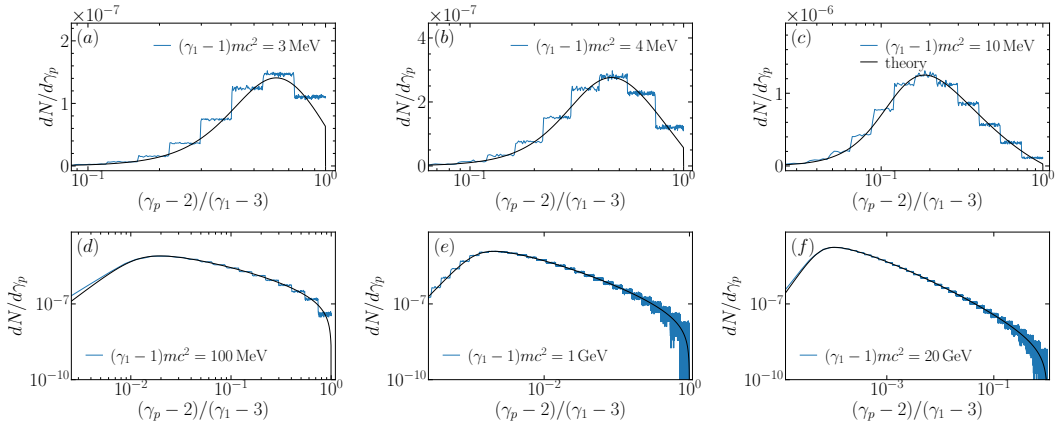

Figure 4: Coulomb Trident pair production in Osiris for different incident electron energies in Copper ($Z = 29$) (a) 3 MeV (b) 4 MeV (c) 10 MeV (d) 100 MeV (e) 1 GeV (f) 20 GeV.

References

[1] B. Martinez, "Radiative and quantum electrodynamic effects in ultra-relativistic laser-matter interaction," Ph.D. dissertation, University of Bordeaux, Dec 2018. [Online]. Available: http://inis.iaea.org/search/search.aspx?orig_q=RN:52022067

[2] B. Martinez, M. Lobet, R. Duclous, E. d'Humières, and L. Gremillet, "High-energy radiation and pair production by Coulomb processes in particle-in-cell simulations," *Physics of Plasmas*, vol. 26, no. 10, p. 103109, 10 2019. [Online]. Available: https://doi.org/10.1063/1.5118339

[3] W. Heitler, *The Quantum Theory of Radiation*, ser. Monographs on Physics. Oxford University Press, 1954.

[4] G. Elwert, *Verschärfte Berechnung von Intensität und Polarisation im kontinuierlichen Röntgenspektrum.* Annalen der Physik, 1939.

[5] S. M. Seltzer and M. J. Berger, "Bremsstrahlung spectra from electron interactions with screened atomic nuclei and orbital electrons," *Nucl. Instrum. Methods Phys. Res. B*, vol. 12, no. 1, pp. 95 – 134, 1985. [Online]. Available: http://www.sciencedirect.com/science/article/pii/0168583X85907074

[6] H. A. Bethe and N. F. Mott, "The influence of screening on the creation and stopping of electrons," vol. 30, p. 524, 1934.

[7] H. W. Koch and J. W. Motz, "Bremsstrahlung cross-section formulas and related data," vol. 31, pp. 920–955, Oct 1959.

[8] J. W. Motz, H. A. Olsen, and H. W. Koch, "Pair Production by Photons," vol. 41, pp. 581–639, Oct 1969.

[9] F. Salvat and J. M. Fernández-Varea, "Overview of physical interaction models for photon and electron transport used in monte carlo codes," *Metrologia*, vol. 46, no. 2, pp. S112–S138, mar 2009. [Online]. Available: https://doi.org/10.1088%2F0026-1394%2F46%2F2%2Fs08

[10] I. B. Vodopiyanov, J. R. Dwyer, E. S. Cramer, R. J. Lucia, and H. K. Rassoul, "The effect of direct electron-positron pair production on relativistic feedback rates," vol. 120, pp. 800–806, Jan. 2015.

[11] Gryaznykh, D. A. and Kandiev, Ya. Z. and Lykov, V. A., "Estimates of electron-positron pair production in the interaction of high-power laser radiation with high-Z targets," vol. 67, no. 4, pp. 257–262, 1998.

[12] V. N. Baĭer and V. S. Fadin, "Electroproduction of Pairs of Particles at High Energies," *Sov. Phys. JETP*, vol. 34, p. 253, 1972.

[13] O. Embréus, L. Hesslow, M. Hoppe, G. Papp, K. Richards, and T. Fülöp, "Dynamics of positrons during relativistic electron runaway," *Journal of Plasma Physics*, vol. 84, no. 5, Oct. 2018. [Online]. Available: http://adsabs.harvard.edu/abs/2018JPlPh..84e9006E

[14] J. Myatt, J. A. Delettrez, A. V. Maximov, D. D. Meyerhofer, R. W. Short, C. Stoeckl, and M. Storm, "Optimizing electron-positron pair production on kilojoule-class high-intensity lasers for the purpose of pair-plasma creation," vol. 79, p. 066409, Jun 2009.

[15] H. J. Bhabha, "The creation of electron pairs by fast charged particles," vol. 152, no. 877, pp. 559–586, 1935.